PARTICLE TRACKING ANALYSIS OF A ROTOR IN GROUND EFFECT

Federico Rovere, [1] George N. Barakos, [2] René Steijl [3]
CFD Laboratory, School of Engineering, University of Glasgow, G12 8QQ, U.K.
www.gla.ac.uk/cfd

Abstract

Computational fluid dynamics (CFD) is used here to predict the behaviour of ground particles, uplifted by a two-bladed rotor. The main focus is to define a safety area where the presence of particles can be considered safe, and compare this area with other distance based criteria. Using data of three different aircraft, scaling factors have been used to take into account the different size of the small-rotor studied and real case scenarios. The results show how heavier helicopters may generate the most dangerous situations, in terms of presence of particles in a delimited area. Furthermore, parallel strategy is analysed, code performances are compared in terms of number of particles computed and amount of processors used for calculations.

Nomenclature

Latin

a	Speed of sound, m/s
B	Ballistic Coefficient, kg/m^2
c	Blade chord, m
C_Q	Rotor torque coefficient, $C_Q = 2Q/\rho_\infty V_{tip}^2 \pi R^3$
C_T	Thrust coefficient, $C_T = 2T/\rho_\infty V_{tip}^2 \pi R^2$
D	Rotor diameter, m
d_p	Particle diameter, m
FoM	Figure of merit, $FoM = C_T^{3/2}/2C_Q$
g	Gravitional acceleration, m/s^2
M	Mach number, $M = V_{tip}c/a_\infty$
N_b	Number of blades
Q	Rotor torque, $N \cdot m$
R	Rotor radius, m
r	Radial coordinate along blade span, m
Re	Reynolds number, $Re = V_{tip}c/\nu_\infty$
S_{rotor}	Rotor disk area, m^2
T	Rotor thrust, N
U	Velocity x-component, m/s
u^*	Friction velocity, m/s
V	Velocity y-component, m/s
v_{max}	Highest value of velocity radial component
V_{rad}	Velocity radial component, $V_{rad} = Ucos(\Psi) + Vsin(\Psi), m/s$
W_{MTOW}	Weight at maximum take-off weight, N

Greek

λ_i	Hover induced velocity, $\lambda_i = \frac{\sqrt{(C_T)}}{2}$
ν	Kinematic viscosity, m^2/s
Ω	Rotor angular velocity, rad/s
Ψ	Local azimuth angle, deg
ρ	Density, kg/m^3
τ_w	Wall shear stress, kg/ms^2
θ	Collective pitch at three-quarter radius, deg

Super and sub scripts

∞	Freestream value
fs	Full-scale
p	Particle
ss	Small-scale
tip	Blade tip value

Acronyms

CFD	Computational Fluid Dynamics
DVE	Degraded Visual Environment
IGE	In Ground Effect
$MTOW$	Maximum TakeOff Weight
$MUSCL$	Monotone Upstream Centred Schemes for Conservation Laws

[1] PhD Student - federico.rovere@glasgow.ac.uk
[2] Professor - george.barakos@glasgow.ac.uk - corresponding author
[3] Senior Lecturer - rene.steijl@glasgow.ac.uk

OGE	Out of Ground Effect
PIV	Particle Image Velocimetry

1 INTRODUCTION

The interaction between the lifting rotor wake and a sediment bed may cause uplift of particles, like sand, dust, snow and even small rocks. This phenomenon is called brownout in case of sand and dust, and whiteout in presence of water droplets and snow. Both phenomena may afflict helicopters in hover and taxiing. The entrained particles are advected by the air flow and may collide with the aircraft structure. Their impact can generate erosion and damages to the structure, and also they can be ingested by the aircraft engine leading to performance reductions. Despite the importance of erosion effects, the most dangerous consequence of brown and whiteout is the degradation of the pilots' visual environment. At certain flight and environmental conditions, the entrained particles may generate a cloud all around the aircraft. In these conditions of Degraded Visual Environment (DVE), the cloud causes a reduction of the pilot visibility and increases the risk of impact with a ground object. Brownout is one of the most dangerous scenario that a helicopter may occur during an IGE operations. In recent years, efforts were made to help pilots by developing sensors and advanced cockpit displays. Dynamic rollover and collisions with objects are common accidents due to the lack of visibility [1]. US Air Force lost 30 special operation aircraft and 60 crew members lost their lives during landing in desert environments since 1990 [2]. In the same report, authors specify that brownout cost to US services is estimated at $100M/yr. Other NATO members experienced similar statistics. UK had 24 brownout mishaps in the period 2005-2009. The German defence force had more than 30 accidents due to dust and snow [2]. The occurrence of brownout is the most common cause of human factor mishaps during military operations [3]. Rotor wakes have a key role in the brownout cloud development, furthermore they can be a source of risks for ground personnel, equipment and landscape due to the forces generated by high outflow velocities. Risks related to wake encounters and the FAA safety separation criteria are widely discussed in [4]. For these reasons, rotor wakes IGE have been studied in depth in past years following different approaches, from full-scale aircraft [5], to small-scale isolated rotors [6, 7]. In the first case, during experiments, the operational scenario it is fully replicated using full-scale aircraft in different scenarios, taking measurements during aircraft flight. [8] [5]. In general, however, measurement techniques used in full-scale experiments, lack high resolution, and cannot provide a detailed view of the phenomena involved. On the other hand, small-scaled studies can be performed in a laboratory, within a controlled environment. Particle Imagine Velocimetry (PIV) and other high resolution measuring techniques are widely used during these studies. However, due to the limited size of the rotors, Reynolds number and Mach number are lower with respect to the full scale case, leading to some differences in the flowfield behaviour.

In the present work, computational fluid dynamics (CFD) has been used to predict the flowfield around a micro two-bladed rotor operating IGE. The test case simulated was experimentally investigated by Lee et al. [6]. Experimental results have been used to full validate CFD results in terms of rotor performance and outflow velocities. The full test case validation is contained in previous works [9] [10]. The outflows produced were used to evaluate particle uplift and particle tracking. To obtain realistic full-scale scenarios, a scaling factor has been applied to flowfield velocities. Three different aircraft data have been used, categorized in terms of weight. Considering the uplift area of particles, and their path it is possible to define safe zones where it was possible to consider the presence of the particles as negligible. Existing safety separation criteria can then be tested. A possible separation distance is suggested by FAA for wake encounters [11] [4]. In that case, a distance of 3 rotor diameters is suggested to allow the dissipation of the wake generated by a rotor in hover or taxiing. Investigations are conducted to verify if the same distance can be considered safe for the presence of particles in the area that can spoil the pilot view of a near aircraft or hit people operating inside the 3 rotor diameters area. All CFD simulations have been performed using the HMB3 (Helicopter Multi-Block) CFD solver of Glasgow University.

2 NUMERICAL MODELS

2.1 CFD SOLVER

HMB3 (Helicopter Multi-Block) [12, 13] is the solver used for all CFD simulations in this work. It solves the Unsteady Reynolds Averaged Navier-Stokes equations (URANS) in integral form with ALE formulation (Arbitrary Lagrangian Eulerian) for time-dependent domains (moving boundaries). URANS equations are discretized using a cell-centred finite volume approach on a multiblock structured grid. HMB3 uses the Osher [14] and Roe [15] approximate Riemann solvers to evaluate the convective fluxes. The viscous terms are discretized using second order central differencing. Third order accuracy in space is provided by the Monotone Upstream Centred Schemes for Conservation Laws (MUSCL) [16]. To avoid non-physical spurious oscillations where large gradients are in-

volved in computations (kile shockwaves), HMB3 uses a modified form of the Albada limiter [17]. An implicit dual time stepping method is employed to perform the temporal integration. Oversets grids (used in this work) [18] and sliding plane [19] methods are available in HMB3 to allow for the relative motion between mesh components, representing ground and rotor blade. Various turbulence models are available in HMB3, including one-equation, two-equation, three and four equations turbulent models. Large-eddy Simulation (LES), Detached-Eddy Simulation (DES) and Delay-Detached-Eddy Simulation (DDES) can also be used with HMB3. For this study two different turbulence model have been used: $k-\omega$ and $k-\omega$ SST [20], furthermore due to the low Reynolds numbers of the test cases a small number of laminar simulations were also performed.

2.2 SCALING THE FLOWFIELD

Analysing flowfield velocities generated by a small-scale rotor is not possible for safety purposes. They are simply too low and harmless to generate any kind of hazards. For this reason, two scaling factors have been applied to flowfield velocities. The first scaling is necessary to obtain values comparable to full scale rotor wake velocities. The second is used to take into account the difference in thrust coefficient of the small and full scale scenario. The blade tip velocity has been used as first scaling factor, which is listed in table 1 for full scale rotors. For the second scaling factor the hover induced velocity has been taken into account. In general, the hover induced velocity is a common reference value for outflow velocities. When it is scaled with V_{tip}, the hover induced velocity is expressed as $\lambda_i = \sqrt{C_T}/2$. The scaled rotor thrust coefficient obtained by the simulation of the micro rotor is $C_T^{ss} = 0.03$, while the C_T^{fs} can be obtained by the aircraft data. Assuming the aircraft in hover flight, and thrust equal to the weight, which is considered the maximum at take off. W_{MTOW}, V_{tip}, and S_{rotor} are specified in table 1, while for the acceleration of gravity and for the air density the following values have been assumed: $g = 9.81 m/s^2$ and $\rho_{air} = 1.225 kg/m^3$.

$$C_T^{fs} = \frac{2W_{MTOW}}{\rho_{air} V_{tip}^2 S_{rotor}}. \tag{1}$$

It is possible, taking into account the effect of the different thrust coefficient to scale the velocities using the ratio of hover induced velocity between full-scale and small-scale cases. The scaling factor obtained is $\sqrt{\frac{C_T^{fs}}{C_T^{ss}}}$. This way, it is possible to estimate the outflow velocities generated by a full-scale rotor operating at the same high values of thrust coefficient of the scaled rotor. The final scaling factor increases the value of the velocities involved in the simulations, due to the stronger influence of the higher rotor tip velocity. It is important to say that this kind of scaling cannot fully represent the complexity of the phenomena involved. This approach do not take into account the different Reynolds numbers that are involved in full and small scale rotors, which may deeply change the wake and its development in time.

2.3 PARTICLE TRACKING

In general, all kinds of particles can be simulated such as rain, ice, sand, and even small rocks. To properly simulate the behaviour in the flowfield it is necessary to model their motion. There are basically two approaches for the numerical simulation of dispersed phases, and they can be categorized into Lagrangian tracking or Eulerian modelling approaches. In the Lagrangian approach, the particles (or parcels of particles) are tracked through the field. For methods that involve this approach the motion of the particles is tracked solving the Newton's second law. Important works in Lagrangian frame of reference are [21] [22]. In the case of Eulerian methods, the properties of the particles are assumed to be continuous within the field. Thus, differential conservation equations are written, discretized, and the solution of these gives the properties of the cloud (size, number of particle involved, density etc.). The Eulerian formulation can be based on number of particles density, [23], or on solid mass particle density [24]. A particle tracking tool has been developed for this work. A pick-up model, based on threshold velocity, has been used to analyse the particle uplift from the ground. Using this information, it was possible to properly seed the ground and track the particles in the flowfield.

2.3.1 PARTICLE UPLIFT

When the wake reaches the ground and interacts with the loose sediment, particles can be uplifted. The Bangold model (see [25, 26]) has been used to simulate brownout in several works. It has been developed within the sediment community to simulate the pick-up of particles in river flows. In 2000 Shao et al. [27] proposed a simple formulation for particles pick-up, based on Bangold model, that has been used in this work. It is a threshold model, based on the wall friction velocity $u_* = \sqrt{\frac{\tau_w}{\rho}}$. The threshold value is function of particle and fluid proprieties and on the gravity. It is computed as:

$$u_t^* = \sqrt{A(\frac{\rho_p}{\rho_{air}} g d_p + \frac{\beta}{\rho_{air} d_p})}, \tag{2}$$

where u_t^* is the threshold velocity, while A and β are coefficients: A=0.0123, β=0.0003 $\frac{kg}{s^2}$. The particle values, used in this work, are listed in Table 2, while for air and gravity the following values have been used: $\rho_{air} = 1.225kg/m^3$ and $g = 9.81m/s^2$. When $u^* > u_t^*$ the particle is uplifted and it is entrained the flowfield. Another cause of particle uplift is "splash entrainment". Anytime an entrained particle hits the ground, it may have sufficiently high energy to launch more particles. The kinetic energy gained by the hit particles can overcome the cohesive forces and lead to uplift. This phenomenon has not been taken into account in the present simulations, but it is described in [28] and [27].

2.3.2 PARTICLE TRACKING METHOD

The particles are driven by the flowfield velocities and their positions in time are obtained by integrating their equations of motion. The integration method used is a forth order Runge-Kutta, and the equation for particle tracking acceleration is.

$$\boldsymbol{a}_p = \frac{0.5\rho_{air}(\boldsymbol{u} - \boldsymbol{u}_p)||(\boldsymbol{u} - \boldsymbol{u}_p)||}{B} - \boldsymbol{g} \tag{3}$$

Where $\boldsymbol{a}_p$ is the acceleration of the particle, $\boldsymbol{u}_p$ is its velocity, $\boldsymbol{u}$ is the velocity of the flowfield in the position of the particle and B the ballistic coefficient, $B = \frac{m_p}{S_p C_D}$. Here m_p is the particle mass, $S_p = \pi d_p^2/4$ is the particle frontal area (particles are assumed spherical) and C_D the particle drag coefficient, and finally **g** is acceleration of gravity. The particle proprieties used in this work are listed in table 2, they reflect the size and the density of particles used to simulate brownout in experimental and computational works [29] [30] [31]. Particle tracking computations have been performed solving the described equations in dimensioneless form. The reference values for length was c, rotor aerodynamic chord. For density was free-stream dendity rho_{inf}, and for velocity was rotor tip velocity V_{tip}.

2.4 PARALLEL COMPUTATION

The particle tracking method was developed to run in serial and in parallel. In parallel, the total amount of particles is divided among the processors. This way, every particle is associated to a processor, which tracks it for the duration of the simulation. The flow chart of the algorithm is presented in Figure 1. First, the method reads the CFD mesh and input file, which contains information about particle proprieties (density, radius, drag coefficient), seeding starting positions, flowfield information (Reynolds number) and gravity. Then, it reads the flowfield files, and releases the particles. Processors do not exchange information about particles, they track their particles from the first timestep to the end of the simulation. After generating additional particles, every processor searches and updates the position of every particle that is associated to it. Finally, every processor writes an output file containing all particle positions at the timestep, which are later postprocessed in a single file. The total execution time is shown in Fig 2 (a) for 100 rotor revolutions, using different numbers of seeding particles, and different number of processors. The results show, as expected, a linear behaviour. The execution time increases with the number of seeding particles tracked, however the linear slope reduced with the number of processors used. All processors track the same number of particles, improving the performance linearly with the number of processors used. A coarser mesh has been used for these results (1.6 M). In Figure 2 (b) the speed up of the total execution time is compared with the ideal linear behaviour. In an ideal parallel strategy, the speedup of a process running in parallel grows linearly with the number of processors. Results show that the particle tracking timing is closer to the ideal case when a smaller amount of processors is used, this is in accordance with the Amdahal's law. [32]. In Fig 2 (b) it is also possible to compare the speed-up of different tests, with different number of seeding particles. When the number of particles is larger, the timing behaviour is slightly closer to the ideal case with respect to the case with a lower amount of seeding particles. Considering a fixed number of revolutions, the serial part of the code does not change with the amount of particles, on the other hand the parallel part increases with it, resulting in better performances with increasing number of processors.

3 COMPUTATIONS AND SAFETY CONSIDERATIONS

Previous works show the detailed validation of our tools for this test case in OGE [10] and IGE [9]. IGE configuration the rotor was modelled using two overset grids, and the ground was modelled imposing no-slip conditions. The full rotor domain was computed as unsteady. The unsteady time step was changed during the simulation, starting with a big timestep which was gradually reduced reaching 0.5deg/timestep for the last revolutions performed. Simulations performed in total 5 full revolutions. The mesh has been refined near the ground and the rotor to accurately resolve the wake features. Three different rotor heights above ground were tested: h/R=0.5, h/R=1 and h/R=1.5, all of them with collective $\theta = 12deg$. Full comparison of performance and outflow results can be found in [10] and [9]. Uplift of particles is shown in figure 3. The computed shear stress on the ground of the domain allowed to calculate the particle velocity uplift threshold. In general, results showed that the peak of the

uplift ratio u_t/u_t^* was in proximity of 1 R distance from the rotor, and the area of uplift particles for the cases considered was at least between 1R and 2R. Heavier helicopters produced stronger outflow, which may extend the uplift area up to 3R. The rotor distance from the ground had a key role in defining the area where particles may be uplifted. Results showed that when the rotor was operating at h/R=0.5, the particles could be uplifted up to a 3 rotor radius distance, while for higher rotor altitude the uplift area could be delimited around 2R. Figure 4 shows results for particle tracking. Seeding points had been realised in proximity to the ground, between 1 and 2R. A new particle was realised in the flowfield form the ground every 5deg of rotor rotation. The full simulation involved 100 revolutions (about 30 seconds of flight for a full scale rotorcraft). Due to the high computational cost of the CFD simulation, the last revolution performed had been considered periodic, and it had been repeated for the full duration of the particle tracking. When the rotor was operating at h/R=1, the particles were uplifted by the flowfield, and then moved away from the rotor, following the radial direction. Particles were driven by the outflow that pushed them away from the rotor. However, depending on the strength of the outflow they reached different positions. Heavy weight helicopters had a stronger outflow, and in this case, particles could reach a maximum radial distance of 8.5R, and a maximum height above the ground of 1R. Once the particles reached the maximum altitude value, they fell again on the ground. Lighter weight helicopter cases, showed lower values for maximum h/R and r/R, however particles went further the 3D separation criteria for wake encounters. A similar path was followed in the case of h/R=1.5, where the particles reached a maximum height of h/R=1.5 for the heavy weight aircraft case. As for the previous case, the maximum height was reached at r/R=6, however the flowfield seemed weaker with respect to the previous case, particles reached a maximum radial distance of 8R, in the most dangerous scenario. On the other hand, when the helicopter was operating at h/R=0.5 particles showed a different behaviour. Initially, particles were uplifted from the ground, then two main branches spreaded, following different paths. Some of them, were reingested by the rotor, reaching the highest distance from the ground. These particles can be dangerous for the crew and the aircraft. The rest of the particles keep following the radial direction far from the rotor, and fall again on the ground at distance around 6.5R for the heavy scale helicopter. Particles that moved away from the rotor can be dangerous for ground personnel and equipment, while the recirculation of the particles creates risks for the helicopter and the crew itself. During the re-ingesting phase particles can hit blades and fuselage and they create the cloud that degrades the visual of the pilot, creating a dangerous DVE condition. The DVE condition is clear in figure 4. These cloud plots can only be compared in a relative sense, because only few positions of the ground have been seeded with particles. In a real brownout scenario, particles can be uplifted from all over the ground where the outflow is strong enough, and their realising time would be shorter than what used in these simulations. All of this will lead to higher dust density concentration. Comparing the obtained results, it is clear that the cloud generated in the case of h/R=0.5 was more severe than the other two cases, due to reingestion of particles, in this case the visibility of the pilot was limited by the high amount of particles in proximity of the rotor disk. On the other hand, when the rotor was operating at h/R=1.0 and h/R=1.5 the higher of cloud densities were confined near the ground in proximity the rotor disk. In this scenario, the pilot had good visibility by an area of aproximately 3 rotor radius, however beyond the 3R distance the cloud started to propagate reaching up to 8R. This scenario may lead to dangerous situations for other aircraft operating in the same area, spoiling other pilots visual or damaging aircraft structures and equipment. The current results show that after 100 revolutions some particles paths are closed. As previously described, some particle fell again on the ground, while other were reingested by the rotor flow. In both cases, however, after this period of time the cloud stops spreading, reaching its maximum distance.

4 CONCLUSION AND FUTURE STEPS

Particle tracking results show that particles can reach large distances away from the rotor, exceed the limit of 3D. In general, it seems that the FAA limit for wake encounters cannot guarantee safety in presence of particles on the ground. It is also clear that to define a particle free zone , it is necessary to take into account the rotor operating conditions due to the strong influence of the disk loading and in general of the size of the aircraft on the particle paths. Particle paths are also strongly influenced by the position of the rotor with respect to the ground. In this work, to obtain full-scale particle paths, scaling factors are applied to a small-scale rotor, however, the full physics of the brownout cannot be simulated in this way, due to the several factors. In general, the Reynolds number that is involved in the small and the full-scale scenario is dissimilar, leading to differences in the uplift phenomena and to a different evolution of the brownout cloud. This study can be a starting point for evaluating safe operational zones around a helicopter. Future work will look at different test cases, with a rotor geometry more similar to full scale rotors, and higher Reynolds number, to

obtain results closer to operational scenarios. Results will be compared with distance safety regulations like the 3 rotor diameters separation distance for wake encounters suggested in the Manual of Air Traffic Service described previously. [11] [4]. Another future step of this research is to use a bombardment model in the particle tracking tool, and analyse its influence in the cloud density development.

5 ACKNOWLEDGMENTS

This project has received funding from the European Union's H2020 research and innovation programme under the Marie Sktodowska-Curie grant agreement No 721920

Results were obtained using the EPSRC funded ARCHIE-WeSt High Performance Computer (www.archie-west.ac.uk), the Cirrus UK National Tier-2 HPC Service at EPCC (http://www.cirrus.ac.uk), and the ARCHER UK National Supercomputing Service (http://www.archer.ac.uk).

References

[1] D'Andrea, A. and Scorcelletti, F., "Enhanced numerical simulations of helicopter landing maneuvers in brownout conditions," *American Helicopter Society International 66th Annual Forum Proceedings, Phoenix, AZ*, 2010.

[2] Taskgroup, R., "Rotary-wing brownout mitigation: technologies and training," *Tech. Rep. RTO-TR-HFM-162, NATO Sci. Technol. Org.*, 2010.

[3] Mapes, P., Kent, R., and Wood, R., "DoD helicopter mishaps FY85-05: findings and recommendations," *US Air Force*, 2008.

[4] Garcia-Dorado, I., Aliaga, D. G., Bhalachandran, S., Schmid, P., and Niyogi, D., "Fast Weather Simulation for Inverse Procedural Design of 3D Urban Models," *ACM Transactions on Graphics (TOG)*, Vol. 36, No. 2, 2017, pp. 21.

[5] Silva, M. and Riser, R., "CH-47D tandem rotor outwash survey," *AHS 67th Annual Forum,Virginia Beach, Virginia, USA,*, 2011, p. 221.

[6] Lee, T. E., Leishman, J. G., and Ramasamy, M., "Fluid dynamics of interacting blade tip vortices with a ground plane," *Journal of the American Helicopter Society*, Vol. 55, No. 2, 2010, pp. 22005–22005.

[7] Milluzzo III, J. I. and Leishman, J. G., "Vortical sheet behavior in the wake of a rotor in ground effect," *AIAA Journal*, Vol. 55, No. 1, 2016, pp. 24.

[8] Wong, O. D. and Tanner, P. E., "Photogrammetric measurements of an EH-60L brownout cloud," 2010.

[9] Rovere, F., Barakos, G. N., and Steijl, R., "Brownout Simulations of Model-Rotors In Ground Effect," *MATEC Web of Conferences*, Vol. 314, 2020.

[10] Rovere, F., Barakos, G., and Steijl, R., "CFD validation of a micro-rotor in grond effect," *45th European Rotorcraft Forum, Warsaw*, No. 81, CFAS, 2019.

[11] CAA, "CAP 490: Manual of Air Traffic Services Part 1," 2015.

[12] Steijl, R., Barakos, G., and Badcock, K., "A framework for CFD analysis of helicopter rotors in hover and forward flight," *International journal for numerical methods in fluids*, Vol. 51, No. 8, 2006, pp. 819–847.

[13] Lawson, S., Woodgate, M., Steijl, R., and Barakos, G., "High performance computing for challenging problems in computational fluid dynamics," *Progress in Aerospace Sciences*, Vol. 52, 2012, pp. 19–29.

[14] Osher, S. and Chakravarthy, S., "Upwind schemes and boundary conditions with applications to Euler equations in general geometries," *Journal of Computational Physics*, Vol. 50, No. 3, 1983, pp. 447–481.

[15] Roe, P. L., "Approximate Riemann solvers, parameter vectors, and difference schemes," *Journal of computational physics*, Vol. 43, No. 2, 1981, pp. 357–372.

[16] Van Leer, B., "Towards the ultimate conservative difference scheme. V. A second-order sequel to Godunov's method," *Journal of computational Physics*, Vol. 32, No. 1, 1979, pp. 101–136.

[17] Van Albada, G., Van Leer, B., and Roberts, W., "A comparative study of computational methods in cosmic gas dynamics," *Upwind and High-Resolution Schemes*, Springer, 1997, pp. 95–103.

[18] Jarkowski, M., Woodgate, M., Barakos, G., and Rokicki, J., "Towards consistent hybrid overset mesh methods for rotorcraft CFD," *International Journal for Numerical Methods in Fluids*, Vol. 74, No. 8, 2014, pp. 543–576.

[19] Steijl, R. and Barakos, G., "Sliding mesh algorithm for CFD analysis of helicopter rotor–fuselage aerodynamics," *International journal for numerical methods in fluids*, Vol. 58, No. 5, 2008, pp. 527–549.

[20] Menter, F. R., "Two-equation eddy-viscosity turbulence models for engineering applications," *AIAA journal*, Vol. 32, No. 8, 1994, pp. 1598–1605.

[21] Alfred, J., Celi, R., and Leishman, J. G., "Flight Path Optimization for Brownout Mitigation Using a High-Fidelity Simulation Model," *Journal of the American Helicopter Society*, Vol. 62, No. 3, 2017, pp. 1–15.

[22] Wachspress, D., Whitehouse, G., Keller, J., Yu, K., Gilmore, P., Dorsett, M., and McClure, K., "A high fidelity brownout model for real-time flight simulations and trainers," Vol. 1, 2009, pp. 278–301.

[23] Phillips, C., Kim, H. W., and Brown, R. E., "The flow physics of helicopter brownout," *66th American Helicopter Society Forum: Rising to New Heights in Vertical Lift Technology*, 2010.

[24] Ghosh, S., Lohry, M. W., and Rajagopalan, R. G., "Rotor configurational effect on rotorcraft brownout," *28th AIAA Applied Aerodynamics Conference*, 2010, p. 4238.

[25] Bagnold, R., "The physics of blown sand and desert dunes," *William Morrow & Co., New York*, 1941.

[26] Greeley, R. and Iversen, J. D., *Wind as a geological process: on Earth, Mars, Venus and Titan*, Vol. 4, CUP Archive, 1987.

[27] Shao, Y. and Lu, H., "A simple expression for wind erosion threshold friction velocity," *Journal of Geophysical Research: Atmospheres*, Vol. 105, No. D17, 2000, pp. 22437–22443.

[28] Shao, Y. and Li, A., "Numerical Modelling of Saltation in the Atmospheric Surface Layer," *Boundary-Layer Meteorology*, Vol. 91, No. 2, May 1999, pp. 199–225.

[29] Syal, M., Govindarajan, B., and Leishman, J., "Mesoscale sediment tracking methodology to analyze brownout cloud developments," *66th Annual Forum of the American Helicopter Society, Phoenix, AZ*, 2010, pp. 11–13.

[30] Kutz, B., Günther, T., Rumpf, A., and Kuhn, A., "Numerical examination of a model rotor in brownout conditions," Vol. 4, 2014, pp. 2450–2461, cited By 9.

[31] Tanner, P. E., "Photogrammetric characterization of a brownout cloud," *67th Annual Forum of the American Helicopter Society, Virginia Beach, VA*, 2011.

[32] Amdahl, G. M., "Validity of the single processor approach to achieving large scale computing capabilities," *Proceedings of the April 18-20, 1967, spring joint computer conference*, 1967, pp. 483–485.

[33] "Vertipedia," `https://vertipedia.vtol.org/`, Accessed: 23-09-2019.

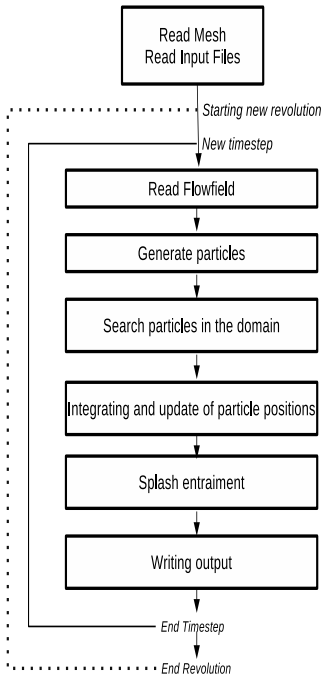

Figure 1: Particle tracking flow chart

Category	MTOW (kg)	R (m)	V_{tip} (m/s)	C_T
Light	3000	5.5	220	0.009
Medium	8000	8.1	216	0.015
Heavy	11000	8.1	220	0.0176

Table 1: Helicopters technical data [33]

$\rho_p(kg/m^3)$	d_p (μm)	C_D	B	u_t^*
2650	9	1.048	0.03	0.58

Table 2: Properties of particles used in this work.

h/R	θ_{75}	C_T	Re_{tip}	M_{tip}
0.5	12deg	0.035	35000	0.08
1.0	12deg	0.03	35000	0.08
1.5	12deg	0.028	35000	0.08

Table 3: Small scale rotor data

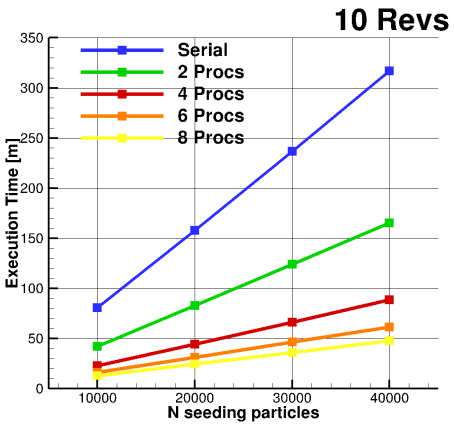

(a) Total Execution time for 10 Revs

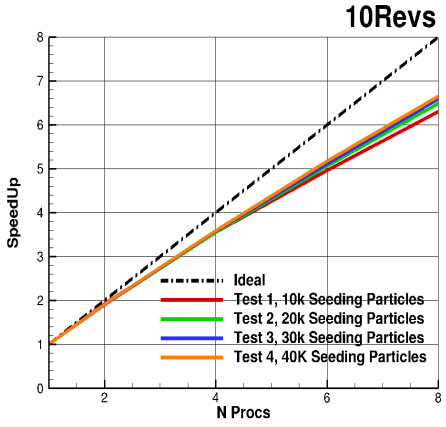

(b) Code and Ideal SpeedUp

Figure 2: Total time for particle tracking

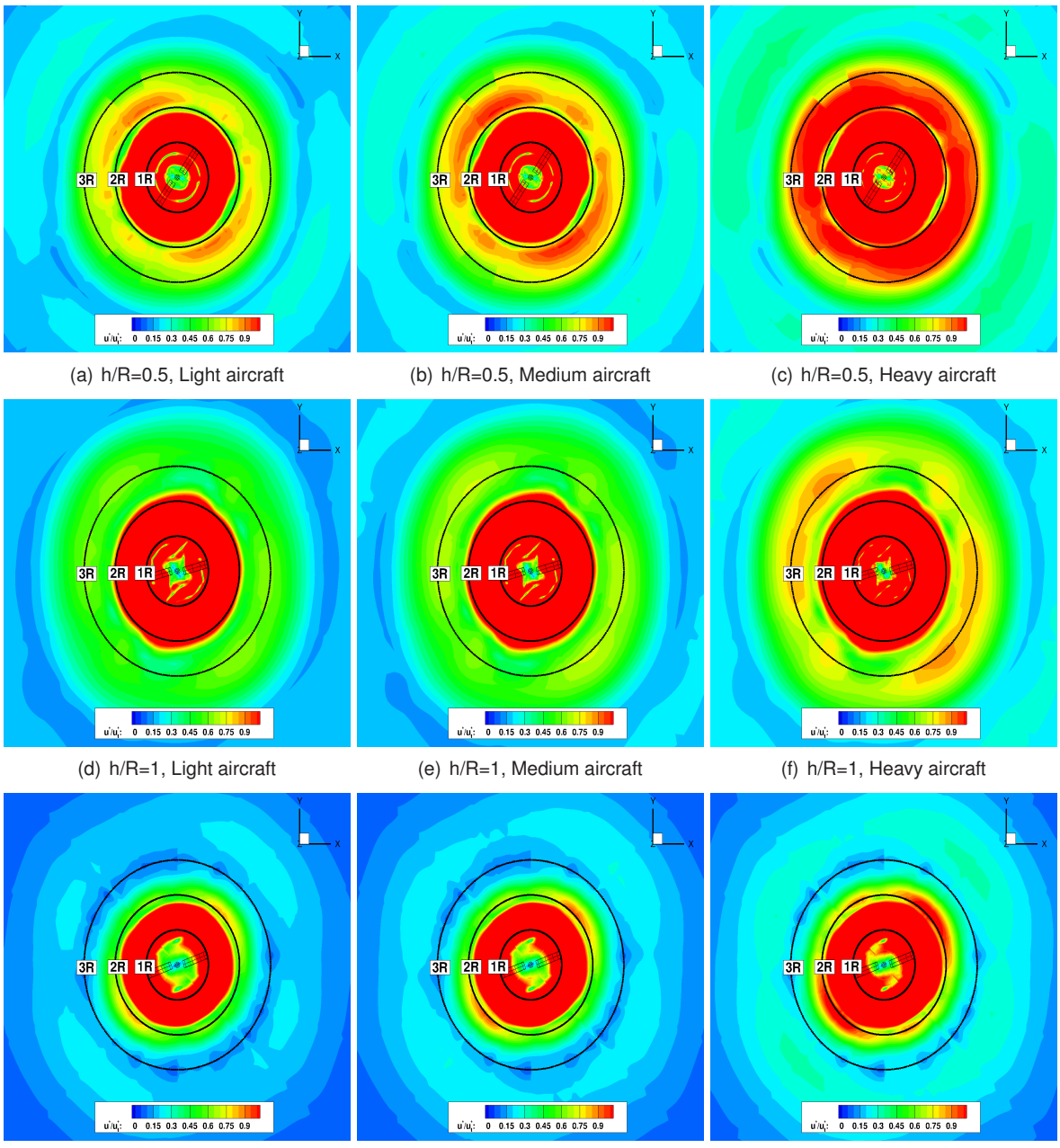

(a) h/R=0.5, Light aircraft (b) h/R=0.5, Medium aircraft (c) h/R=0.5, Heavy aircraft

(d) h/R=1, Light aircraft (e) h/R=1, Medium aircraft (f) h/R=1, Heavy aircraft

(g) h/R=1.5, Light aircraft (h) h/R=1.5, Medium aircraft (i) h/R=1.5, Heavy aircraft

Figure 3: Uplift results for rotor at different heights above the ground and different scaling factors. All operational conditions of the small scaled rotor are listed in table 3.

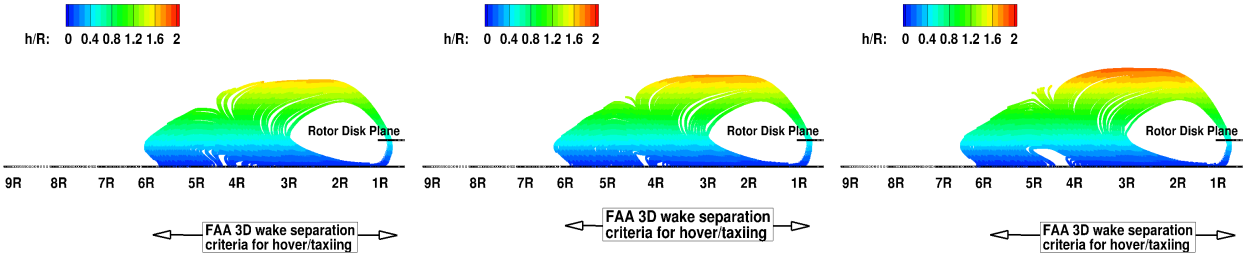

(a) h/R=0.5, Light aircraf (b) h/R=0.5, Medium aircraft (c) h/R=0.5, Heavy aircraft

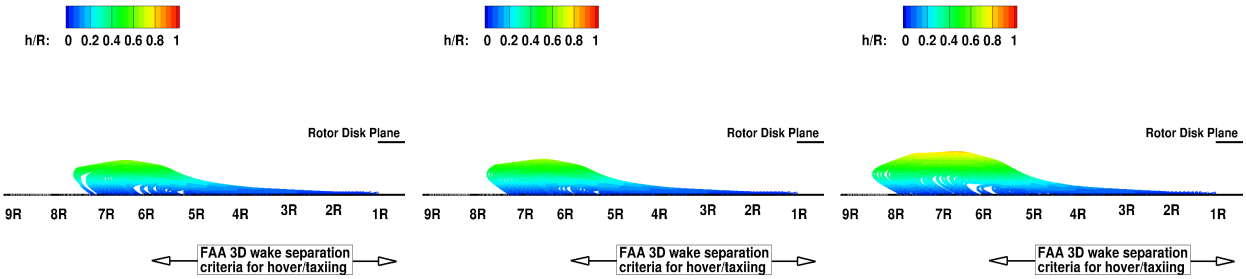

(d) h/R=1, Light aircraft (e) h/R=1, Medium aircraft (f) h/R=1, Heavy aircraft

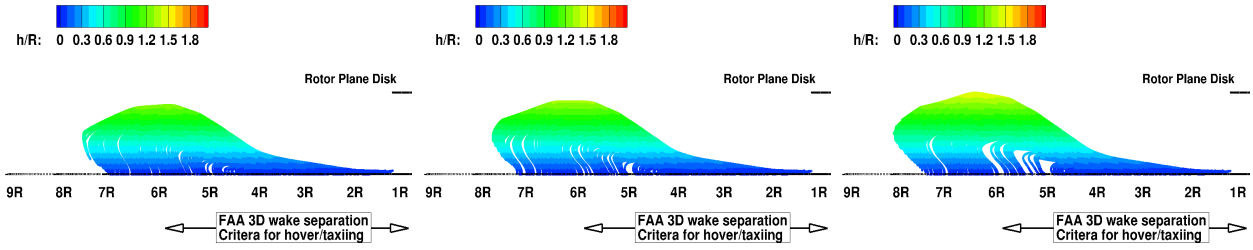

(g) h/R=1.5, Light aircraft (h) h/R=1.5, Medium aircraft (i) h/R=1.5, Heavy aircraft

Figure 4: Particle paths for rotor at different heights above the ground and different scaling factors. All operational conditions of the small scaled rotor are listed in table 3.